

# Hydrogen donation of bio-acids over transition metal facets: A Density Functional Theory study

Jiajun Zhang<sup>ac</sup>, Xiaolei Zhang<sup>ac,\*</sup>, Amin Osatiashtiani<sup>b</sup>, Anthony Bridgwater<sup>b</sup>

\* Corresponding author: X.Z., E-mail address: [xiaolei.zhang@strath.ac.uk](mailto:xiaolei.zhang@strath.ac.uk)

<sup>a</sup> Department of Chemical and Process Engineering, University of Strathclyde, Glasgow, United Kingdom

<sup>b</sup> European Bioenergy Research Institute (EBRI), School of Engineering and Applied Science, Aston University, Aston Triangle, Birmingham, B4 7ET, United Kingdom

<sup>c</sup> School of Mechanical and Aerospace Engineering, Queen's University Belfast, Belfast, United Kingdom

## Abstract

This research aims to evaluate and systematic compare two bio-based acidic hydrogen donors as alternative hydrogen source for hydrodeoxygenation (HDO) of bio-oil from fast pyrolysis of biomass. We investigated the hydrogen donation performance of acetic acid (AcOH) and formic acid (FA) over the most stable facet of transition metal in comparison with the dissociation of H<sub>2</sub>, using Density Functional Theory (DFT) modelling. It was found that AcOH adsorbed more strongly on Mo (110) than the other base transition metals investigated. The binding of both acid molecules and Mo were dominated by electrons migration from the molecule to the metal, while electron enrichment was also observed for FA during the adsorption. The bonds strength for both acids were weakened by Mo, therefore, facilitating their decomposition. The hydroxyl hydrogen and one methyl hydrogen of AcOH could be readily cleaved with low energy barriers, but the methylene hydrogen was found to be difficult to cleave when the carbon was unsaturated. Within

24 the FA molecule, the hydroxyl hydrogen would be donated more readily than the  
25 hydrogen from aldehyde group. H<sub>2</sub> dissociated during adsorption on the Mo (110) facet  
26 with negligible energy barrier. Within the three sources of hydrogen (acetic acid, formic  
27 acid and H<sub>2</sub> gas), H<sub>2</sub> gas has the advantage of easy dissociation when compared to the  
28 hydrogen generated from biomass-derived acids (bio-acids). However, the large  
29 enthalpy change resulted from the exothermic decomposition of the bio-acid will probably  
30 facilitate the activation and further migration of the single H atom for donation over the  
31 metal facet compared to H<sub>2</sub> gas. AcOH exhibited a greater potential than FA as a  
32 hydrogen donor over Mo (110) due to the release of more H atoms with low energy  
33 barriers. The modelling results also suggested that AcOH is a promising alternative  
34 hydrogen source to replace H<sub>2</sub> gas over the facet of Mo (110).

35 **Abbreviations:** Acetic Acid, AcOH; Formic Acid, FA; Aromatic Hydrocarbons, AHs;  
36 Electronic density difference, EDD

37

38 **Key words:** Hydrogen donor compounds; Catalytic decomposition; Hydrodeoxygenation;  
39 DFT modelling; Transition metals

40

## 41 **1. Introduction**

42 Nowadays biofuel is an attractive alternative fuel because it can lower our dependency  
43 on conventional fossil fuels, achieve “zero” net carbon emissions, and tackle the  
44 challenge of global warming [1]. Thermochemical conversion of waste biomass via  
45 catalytic fast pyrolysis offers a promising route to biofuels. However, the direct use of  
46 bio-oil is hindered by its undesirable physicochemical properties such as low calorific  
47 value due to its high oxygen content and water content, high viscosity and low stability  
48 owing to its high acid content. This explains why upgrading is being so intensively studied.

49 Hydrodeoxygenation (HDO) is considered an effective method for upgrading bio-oil to  
50 more valuable and useful liquid products [2]. Conventionally, molecular H<sub>2</sub> gas is used  
51 in industrial HDO processes, because of its dissociation on the surface of the catalysts,  
52 thus providing high reactivity. However, there are some drawbacks associated with the  
53 application of molecular H<sub>2</sub> gas such as the high process costs due to high-pressure  
54 reactors, concerns over process safety regarding H<sub>2</sub> storage and utilisation, the  
55 requirement to recover and recycle hydrogen. Additionally, using pure H<sub>2</sub> during HDO  
56 may lead to the saturation of aromatic rings, producing undesired cycloalkanes instead  
57 of aromatic hydrocarbons. Therefore, alternative sustainable hydrogen sources are  
58 urgently sought-after to address the challenges of developing an efficient and cost  
59 effective HDO process.

60 Much effort has been devoted to finding the alternative hydrogen sources, and it has  
61 been reported that hydrogen can be produced in-situ via various reactions [2,3].  
62 Commonly reported alternative hydrogen donors include primary and secondary  
63 alcohols such as methanol, ethanol and isopropyl alcohol (IPA), carboxylic acids  
64 including acetic acid (AcOH) and formic acid (FA), and aromatic hydrocarbons (AHs)  
65 including tetralin and decalin [4,5]. These hydrogen-rich compounds can supply  
66 hydrogen for the HDO reaction through self-decomposition or dehydrogenation [1]. For  
67 example, Wang et al. [6,7] reported the deoxygenation of phenol over Ni/Al<sub>2</sub>O<sub>3</sub> and Ru  
68 based catalysts using methanol and formic acid as hydrogen donor compounds. Guo et  
69 al. [8] explored the HDO of p-cresol over a Ru based catalyst with IPA as the hydrogen  
70 donor, achieving 98.5% conversion and 84.0% yield of toluene. IPA was also found to  
71 be effective in humins conversion [9]. Vasiliadou and Lemonidou reported the HDO of  
72 glycerol at 220 – 250 °C. The highest 1,2-propanediol yield of 53% was obtained using  
73 ethanol as the source of hydrogen [10]. Pajak et al. [11] investigated the hydrogen  
74 transfer from tetralin and decalin to coal derived tars, revealing hydrogen transfer from

75 decalin was two times greater than that of tetralin. Similar conclusions were drawn by  
76 other researchers when decalin and tetralin were used for bio-oil upgrading through  
77 hydrogen transfer deoxygenation [12,13]. In-situ H<sub>2</sub> gas production can also take place  
78 through redox reactions. For example, water-gas shift reaction ( $\text{CO} + \text{H}_2\text{O} \rightleftharpoons \text{CO}_2 + \text{H}_2$ )  
79 may occur within the HDO process to supply hydrogen [14].

80 The mechanism of various hydrogen transfer reactions for HDO have been extensively  
81 investigated [15–18]. The adsorption and dissociation of molecule hydrogen over various  
82 transition metals were reported by Pozzo et al., indicating Ni was the most effective metal  
83 in such a process [19]. Experimental and modelling investigation performed by Grilc and  
84 Likozar and other researchers revealed that bi-functional Ni-Mo based catalysts are  
85 promising for HDO with molecular H<sub>2</sub> [20,21]. Numerical models have been reported as  
86 well [22–24] to describe the mechanism and kinetics of catalytic HDO reactions.

87 DFT based studies regarding decomposition of bio-alcohols have been also intensively  
88 reported; the decomposition mechanism of methanol over Co(0001) and Co(111),  
89 Pd(111), Pt(111), and Ni(111) facets has been investigated, predicting all the C-H bond  
90 and C-O bond would cleave prior to the CO bond in these scenarios [25,26]. Alcalá et al.  
91 reported the decomposition mechanism of ethanol, predicting that demethylation  
92 reaction would happen much faster than dehydroxylation over Pt(111), and methane and  
93 CO were more likely to be produced [27,28]. In addition, detailed mechanisms for ethanol  
94 decomposition over various transition metals, propanol decomposition over Ni-Fe and  
95 Ni-Cu bimetallic facet, and butanol decomposition over Pd(111) facet have been widely  
96 reported [28–31].

97 There are limited reports on the DFT modelled decomposition of AHs (as H donors). Kim  
98 et al. elucidated the dehydrogenation mechanism of decalin to tetralin and further to  
99 naphthalene on the (111) facet of Pd and Pt respectively, revealing that according to the

100 modelling, Pd would outperform Pt by lowering the energy barrier of tetralin conversion  
101 to naphthalene by 0.31 eV [32].

102 Regarding the bio-acids, the decomposition of FA over Cu (111) facet has been analysed  
103 by DFT, predicting the most favourable reaction pathway was  $\text{HCOOH} \rightarrow \text{HCO} \rightarrow \text{CO}$   
104 [33]. The decomposition of acetic acid over a variety of catalysts were also reported  
105 [34,35]. Xinbao et al. investigated the decomposition mechanism of AcOH over Co (111)  
106 stepped facet, and revealed that the reaction pathway follows  $\text{CH}_3\text{COOH} \rightarrow \text{CH}_3\text{CO} \rightarrow$   
107  $\text{CH}_2\text{CO} \rightarrow \text{CH}_2 \rightarrow \text{CH}$  [36]. Although, there are other different reaction mechanisms for  
108 AcOH decomposition proposed in the literature [37–39]. The detailed description of the  
109 decomposition of bio-acids over different catalysts, especially over base transition metals,  
110 are still unclear and scarce. Moreover, previous studies have reported the performance  
111 of various hydrogen donors, however most of them cannot be compared because  
112 different catalysts were used. There are very few reports on the evaluation of the  
113 reactivity of different hydrogen donor compounds over one selected catalyst and their  
114 capacity for HDO reactions.

115 Hence, this research is aimed at the evaluation and systematic comparison between two  
116 bio-based acidic hydrogen donors, since they abundantly exist in the primary bio-oil. The  
117 decomposition of these carboxylic acids leads to in-situ hydrogen formation, which  
118 subsequently can take part in HDO reactions. With respect to catalyst selection, the  
119 performance of noble metal based catalysts e.g. Pt and Ru, have been widely studied,  
120 while not enough attention have been paid to the base transition metals. Therefore, this  
121 study has sought to predict the decomposition of AcOH with a focus on the cleavage of  
122 hydrogen related bonds over various transition metals. Ten transition metals (Ni, Mo, Fe,  
123 Co, Pt, Rh, Ru, Zn, Cu, and Pd) are compared regarding their binding energy in  
124 adsorbing AcOH and the one with strong binding was selected. Then, AcOH and FA are  
125 compared with  $\text{H}_2$  in terms of their adsorption process and hydrogen donation

126 performance over the most stable facet of the selected catalyst. Electronic density  
127 difference (EDD) of the hydrogen donor compounds was analysed to investigate the  
128 interface interactions. Bond lengths of the donor compounds were also tracked  
129 throughout their decomposition to evaluate the impact of metal catalyst.

## 130 **2. Computational details**

131 The first-principle density functional theory plus dispersion (DFT-D) calculations were  
132 implemented in the Cambridge Sequential Total Energy Package (CASTEP) module  
133 available in Materials Studio 2017 R2 from BIOVIA [40,41]. The generalized gradient  
134 corrected approximation (GGA) [42] treated by the Perdew–Burke–Ernzerhof (PBE)  
135 exchange-correlation potential with long-range dispersion correction via Grimme's  
136 scheme was used to calculate the exchange-correlation energy [43]. The On-the-fly  
137 generated (OTFG) ultrasoft pseudopotential was employed as the scheme in the  
138 representation of reciprocal space for all the elements [44,45]. The plane-wave cut-off  
139 energy was set to 500 eV for all the calculations based on its independence test (Fig.  
140 S1(a)). The Brillouin zone was sampled using a  $2 \times 2 \times 1$  Monkhorst-Pack k-point (spacing  
141 of  $0.04 \text{ \AA}^{-1}$ ) with a smearing of 0.1 eV, based on its independence test (Fig. S1(b)). The  
142 self-consistent field (SCF) tolerance was set to  $10^{-6}$  eV/atom. All the modelling was  
143 performed with a convergence threshold of  $10^{-5}$  eV/atom on energy, 0.03 eV/Å on  
144 maximum force, and  $10^{-3}$  Å on the maximum displacement. No symmetry constraints  
145 were used for any modelling. The impact of zero point energy (ZPE) was evaluated for  
146 the adsorption of AcOH and FA. It was found that the net ZPE corrections (difference  
147 between ZPE of the systems before and after the adsorption) were less than 0.01eV, so  
148 that the ZPE correction was not included in the calculations of this study. The  
149 computational method is believed to give high precision results, according to the  
150 validation of lattice constant for each metal element lattice in this study; the variations

151 between computational and experimental values are less than 0.10 Å for most systems  
152 (full comparison is shown in Table S1).

153 The most stable facets of the ten metals were simulated; facet (1 1 1) was simulated for  
154 face-centred cubic (FCC) metals including Ni, Cu, Pd, Pt, and Rh, and facet (1 1 0) was  
155 simulated for body-centred cubic (BCC) metals of Mo, Fe. For hexagonal close-packed  
156 (HCP) metals including Co, Zn, and Ru, facet (0 0 1) was simulated [28,46]. All the metal  
157 facet models were created from the optimized metal lattices, and a four-layer slab of P  
158 (5×5) super-cell was used with the adsorbate coverage of 1/25ML (Fig. S2). 15Å vacuum  
159 region was created above the metal facet. The transition state (TS) was completely  
160 determined by the LST/QST method, and the TSs for the dominated reaction steps were  
161 confirmed by the unique imaginary frequency. Mulliken charges were assigned to each  
162 bond to address the bond order [47]. The adsorption energy  $E_{ad}$  was determined by Eq.1,  
163 where  $E_{catalyst}$ ,  $E_{adsorbate}$  and  $E_{adsorbate/catalyst}$  are the total energies of clean metal facet, free  
164 adsorbate molecule and metal facet with adsorbed molecule respectively. The energy  
165 barriers of reactions  $E_{barrier}$  were determined by the difference between the transition  
166 state and reactant energies, as shown in Eq.2, where  $E_{transition\ state}$  and  $E_{reactant}$  are the total  
167 energies of the transition state and reactant of a reaction.

$$168 \quad E_{ad} = E_{catalyst} + E_{adsorbate} - E_{adsorbate/catalyst} \quad Eq.1$$

$$169 \quad E_{barrier} = E_{transition\ state} - E_{reactant} \quad Eq.2$$

170 EDD was determined by Eq.3.

$$171 \quad \Delta\rho = \rho_{adsorbate@Mo(110)} - (\rho_{adsorbate} + \rho_{Mo(110)}) \quad Eq.3$$

172 where  $\rho_{adsorbate@Mo(110)}$  is the electron density of the total adsorbate + Mo(110) system,  
173 and  $\rho_{adsorbate}$  and  $\rho_{Mo(110)}$  are the unperturbed electron densities of the adsorbate and the  
174 Mo(110) facet, respectively.

175 Geometry optimization was implemented to every model before energy was calculated.  
176 Energy of all the geometries was calculated at 0K in the DFT investigation.

### 177 **3. Results and discussion**

#### 178 3.1 Metal catalyst selection based on AcOH adsorption

179 Most stable facets of ten transition metals were established to identify the metal catalyst  
180 that can adsorb AcOH more strongly than the others. The adsorption modelling was  
181 carried out by placing AcOH molecule vertically, and binding onto the top site of each  
182 metal facet with the carbonyl oxygen atom. More details of the stable adsorption models  
183 are shown in the Fig. S2. The adsorption energies are summarized in Table 1, along with  
184 relevant geometry parameters (bond length of O-metal, which refers to the distance  
185 between the centres of the bounded oxygen atom and the nearest metallic atom, and  
186 the corresponding angle of C-O-metal) of the most stable geometry.

187 Table 1. Adsorption energies and geometrical parameters of AcOH on common facets  
188 of transition metals

Metal facets	Bond length (Å)	$\angle$ C-O-metal (degree)	Adsorption energy (eV)
Ru (0001)	2.16	143.22	0.91
Mo (110)	2.10	170.16	0.88
Ni (111)	1.93	169.33	0.71
Pd (111)	2.14	141.28	0.70
Fe (110)	1.97	170.92	0.67
Co (0001)	1.95	176.82	0.66



Rh (111)	2.21	175.10	0.60
Pt (111)	2.32	137.75	0.58
Cu (111)	2.15	148.03	0.47
Zn (0001)	2.72	127.95	0.30

189 Note: Considering the effects of adsorption sites and compounds configurations on adsorption energy, more  
 190 comprehensive adsorption energy of AcOH onto the top three metal facets of Ru, Mo and Ni in different  
 191 adsorption sites and configurations are calculated and shown in Table 2 and Table. S2.

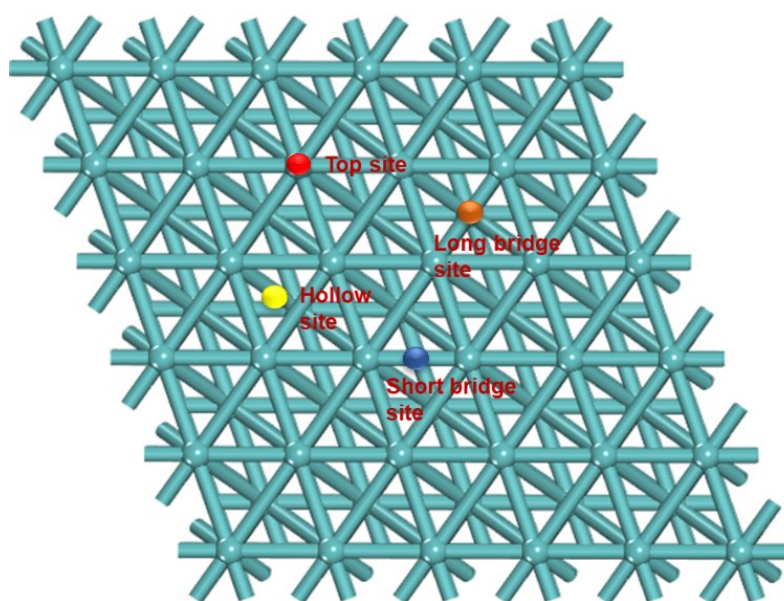
192 The adsorption energy of AcOH onto all of the modelled transition metals facets were  
 193 less than 1.00 eV. The highest adsorption energy of 0.91 eV and 0.88 eV associated  
 194 with AcOH adsorption onto Ru (0001) and Mo (110) respectively, followed by 0.71 eV for  
 195 Ni (111) and 0.70 eV for Pd (111). Adsorption of AcOH on Zn (0001) exhibited the lowest  
 196 adsorption energy of 0.3 eV. The bonds generated between metal facets and AcOH  
 197 molecule ranged from 1.93 to 2.72 Å, and the angles generated between C-O bond and  
 198 O-metal bond ranged between 127.95° and 176.10° for all cases.

199 In the perspective of thermodynamic, the high adsorption energy for Ru, Mo, Ni, Pd  
 200 implies that chemisorption happens with a strong binding between AcOH molecule and  
 201 the metals facets. These four metals are commonly known as the catalysts being  
 202 adopted for the HDO using H<sub>2</sub> gas and for the decomposition of organic compounds with  
 203 good performance [5,48–50]. Specifically for acids decomposition, Ru, Ni and Pd have  
 204 been widely reported based on experimental investigation as well as DFT modelling  
 205 [6,7,34,39,51]. Ru was found quite active in HDO with formic acid as hydrogen donor [7].  
 206 Ni was reported to exert high activity in HDO with H<sub>2</sub> gas but poor performance with  
 207 formic acid as hydrogen donor [6]. Pd is also active but has the potential to lead to the  
 208 direct formation of CH<sub>4</sub> instead of hydrogen donation [34]. Besides, Ru and Pd are noble

209 metals, which would lead to high cost. In comparison, Mo as catalyst has been less  
210 investigated thus it is the focus for the further investigations in this study.

### 211 3.2 AcOH as hydrogen donor on Mo (110) facet

212 The adsorption of AcOH onto Mo (110) facet is investigated in terms of the preferred  
213 absorption sites and configuration. Four probable adsorption sites are considered for the  
214 adsorption modelling, including top site (Top), short bridge site (SB), long bridge site (LB)  
215 and hollow site, as shown in Fig. 1.

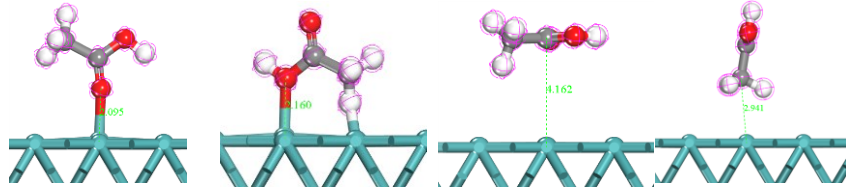


216

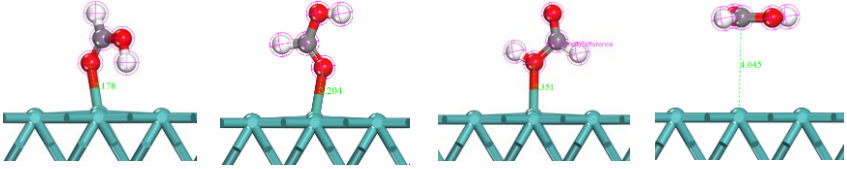
217 Fig. 1. The probable adsorption sites on the facet of Mo (110)

218 The adsorption of AcOH was simulated over four different adsorption sites, and four  
219 configurations for AcOH were compared. The structures of each stable adsorption are  
220 shown in Table 2.

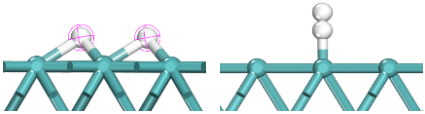
221 Table 2. Adsorption energy of AcOH, FA and H<sub>2</sub> onto Mo (110) at different sites and  
222 configurations

Adsorption Energy of AcOH (eV)				
	① O <sub>α</sub> -Mo	② O <sub>β</sub> -Mo	③ Parallel	④ C <sub>α</sub> -Mo
Top	0.88	0.70	0.28*	0.22*
Short Bridge (SB)	1.24	-	-	-
Long Bridge (LB)	0.28*	-	-	-
Hollow	0.95	-	-	-

Adsorption Energy of FA (eV)				
	① O <sub>α</sub> -Mo	② C-Mo**	③ O <sub>β</sub> -Mo	④ Parallel
Top	1.15	0.75	0.51	0.18*
Short Bridge (SB)	0.15*	-	-	-
Long Bridge (LB)	0.16*	-	-	-
Hollow	0.12*	-	-	-

Adsorption Energy of H <sub>2</sub> (eV)		
	① Parallel	② Vertical
Top	0.57	0.56
Hollow	1.64	-

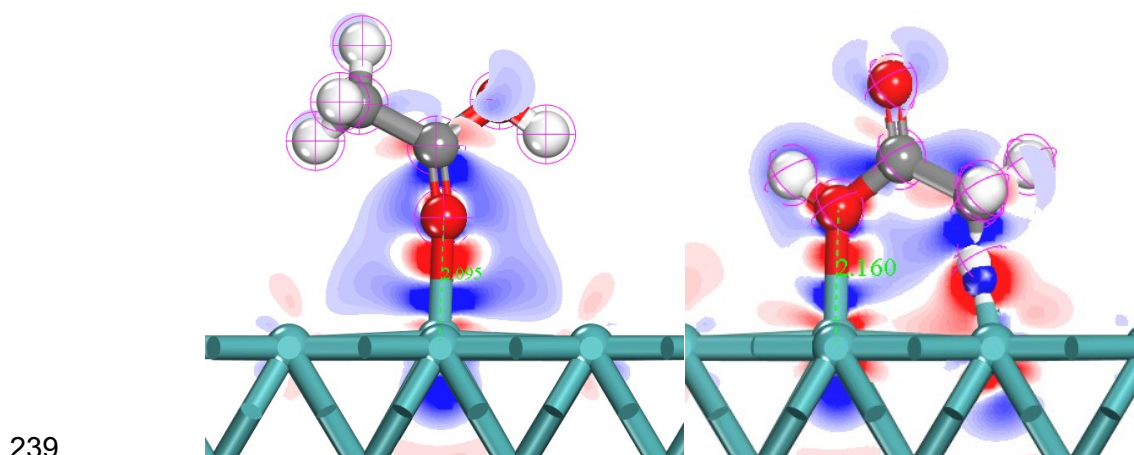
223 \* Only stable physical adsorption observed

224 \*\* Transformed binding from C-Mo to O-Mo (as shown) after geometry optimization

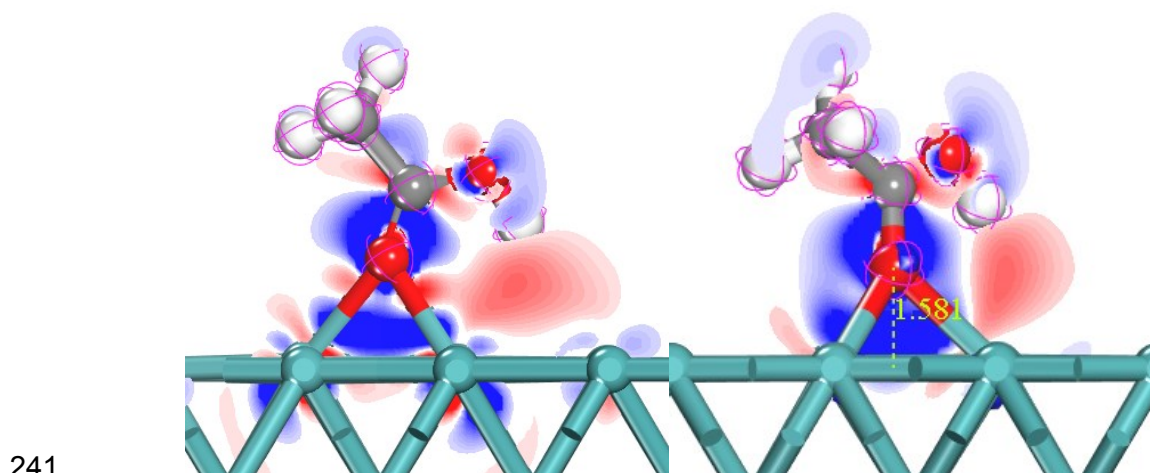
225 Configuration ① led to the highest AcOH adsorption energy of 0.88 eV compared to  
 226 other configurations, followed by configuration ④, for 0.70 eV. While configuration ②  
 227 and ③ resulted in lower adsorption energies of 0.28 eV and 0.22 eV respectively.  
 228 Regarding different adsorption sites based on configuration ①, AcOH was able to  
 229 develop strong bindings on to the top, SB and hollow site of Mo facet, resulting in the

230 adsorption energy of 0.88 eV, 1.24 eV and 0.95 eV respectively. The adsorption of AcOH  
231 onto LB site gave rise to the adsorption energy of 0.28 eV.

232 The results reveal that AcOH molecule most likely will adsorb on the SB site of Mo (110)  
233 facet through the binding between O<sup>a</sup> and Mo facet, leading to the highest adsorption  
234 energy. Carbon and hydrogen in the molecule are found hardly to form strong bond with  
235 the Mo facet independently. The adsorption onto the positions of Top ① and SB ②, and  
236 hollow are likely to be chemical adsorption, because of the large adsorption energy. To  
237 confirm this, electrons migration between the interfaces was investigated by the  
238 calculation of EDD, as shown in Fig. 2.



240



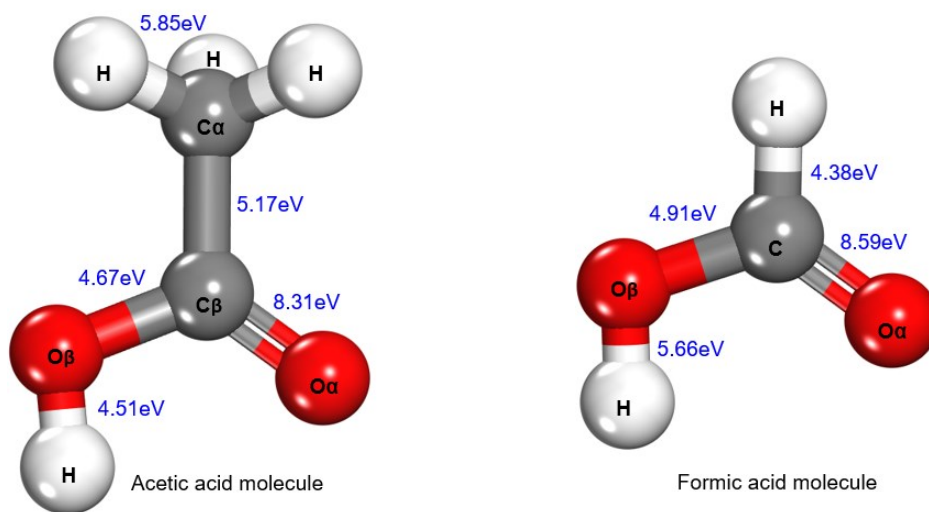
242

243 Fig. 2. Colour mapping of electron density difference (threshold value: +/- 0.05  
244 electrons/Å<sup>3</sup>) for AcOH adsorption configurations of (a) Top ①, (b) Top ②, (c) SB, and  
245 (d) hollow. (Loss of electrons is indicated in blue, while electron enrichment is indicated  
246 in red)

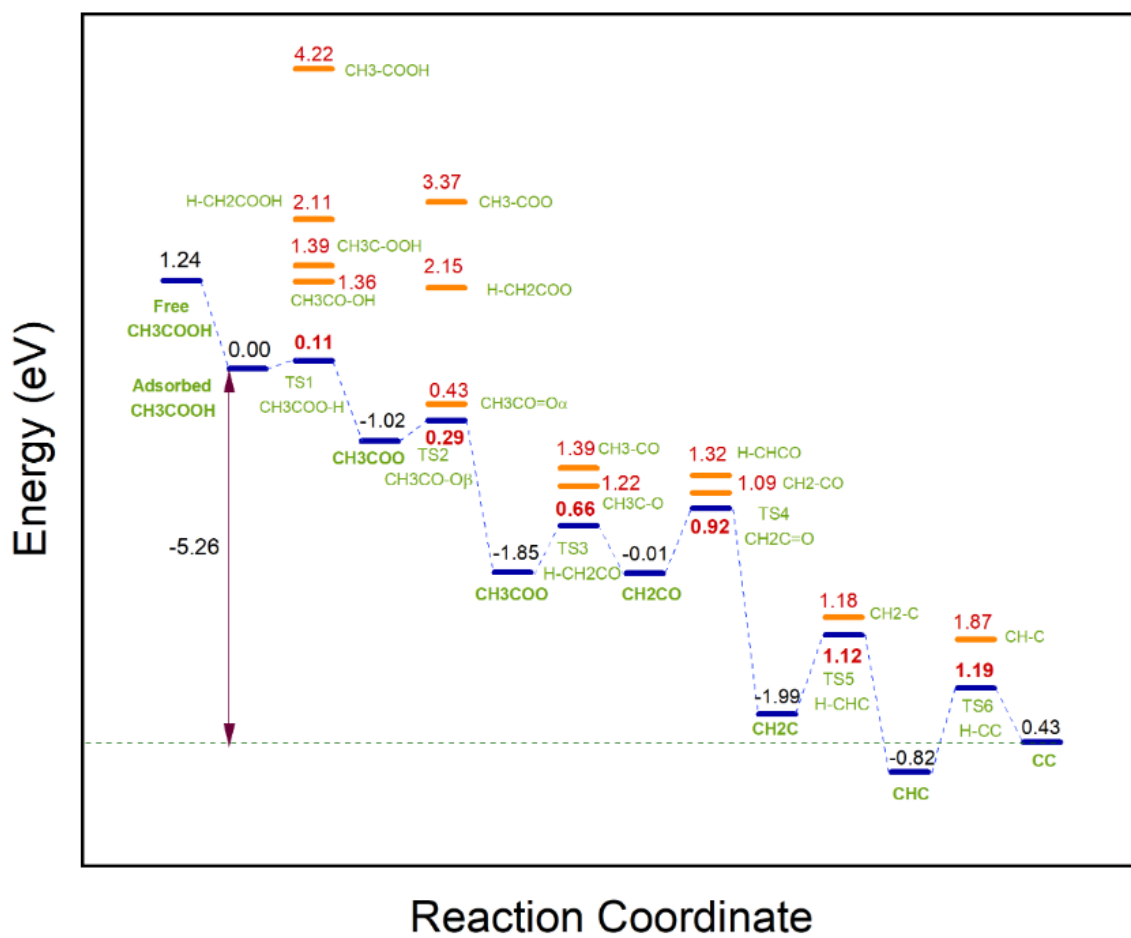
247 Obvious electrons migration around the interfaces of the above four adsorptions  
248 indicates that chemical adsorption happened. The adsorption was likely to happen via  
249 O<sup>α</sup>, where was also the centre for electron migration. When only O<sup>α</sup> atom ( Fig. 2(a) and  
250 (b)) bonded to the facet, fewer electrons were lost but apparent electrons enrichment  
251 was observed around the O<sup>α</sup> atom (Fig. 2(a)) and around the adsorbed hydrogen atom  
252 (Fig. 2(b)). However, severer electron loses happened when AcOH bound to two Mo  
253 atoms through O<sup>α</sup> atom over the SB and hollow positions (in Fig. 2(c) and (d)). These  
254 results are in agreement with the highest adsorption energy on these two sites. They  
255 also reveal that the stable adsorption of AcOH on Mo (110) is achieved by strong electron  
256 migration from the molecule to the substrate through the bridge of C<sup>β</sup>- O<sup>α</sup>-Mo.

257 During modelling the decomposition of AcOH over Mo (110), the cleavage energy and  
258 reaction enthalpy were also calculated, in comparison with the free molecular  
259 decomposition of AcOH molecule in the absence of metal catalyst, which is shown in Fig.  
260 3. The most favourable decomposition pathway of AcOH is illustrated in Fig. 4. The bond  
261 lengths and bond orders for the AcOH molecule and its most probable intermediates  
262 during the decomposition are shown in Table. S3 (a) and (b).

263 For the free molecular decomposition of AcOH, the C<sup>β</sup>-O<sup>α</sup> bond showed the largest  
264 cleavage energy of 8.46 eV, which was followed by the C<sup>α</sup>-H bond with 5.85 eV and the  
265 C-C bond with 5.17eV. The bonds of O<sup>β</sup>-H bond and C<sup>β</sup>-O<sup>β</sup> exhibited similar cleavage  
266 energy of 4.51 eV and 4.67 eV respectively. All the cleavage reactions in free molecular  
267 decomposition were endothermic as there was no new bond formed.



268 Fig. 3. The cleavage energy for the free molecular decomposition of AcOH and FA



269

270

Fig. 4. The decomposition pathways of AcOH over Mo (110) facet

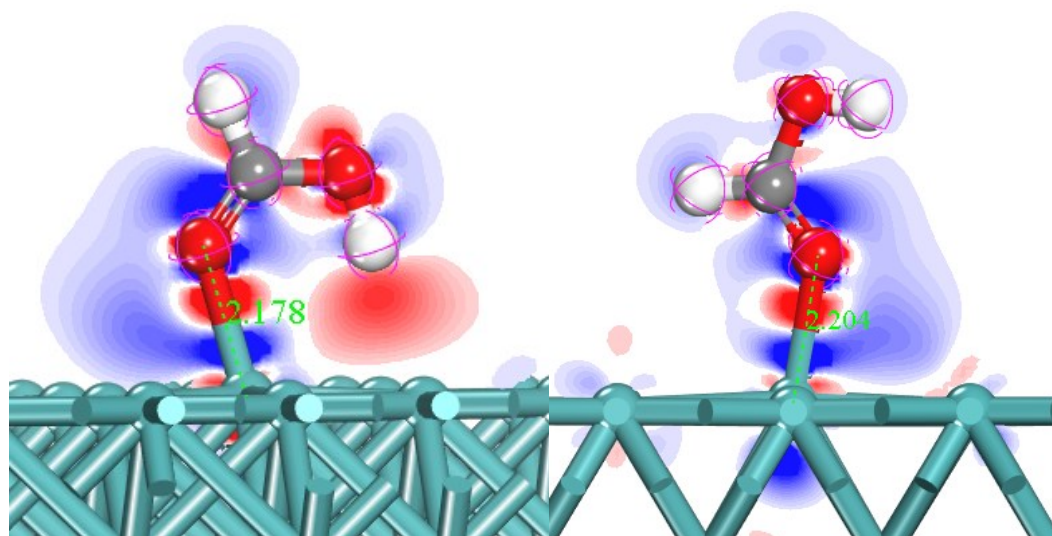
271 The decomposition of AcOH over Mo facet was the most likely to start with the cleavage  
272 of the hydroxyl group with a small energy barrier of 0.11 eV, producing acetate and one  
273 H atom. The acetate could then lose the O<sup>β</sup> atom and one H sequentially to form CH<sub>2</sub>CO.  
274 All the cleavage reactions in the decomposition of AcOH over Mo facet were exothermic,  
275 except for the final H-CC cleavage step, which was endothermic with ΔH = 0.43 eV.

276 The reaction modelling results reveal that the bulk decomposition of AcOH over Mo (110)  
277 is exothermic, which is much more thermodynamically favoured compared to its free  
278 molecular decomposition. Besides, the significant decrease in cleavage energy  
279 observed during the catalytic decomposition indicates the excellent effect of Mo facet in  
280 facilitating the cleavage of AcOH. The most favourable decomposition pathway of AcOH  
281 over Mo (110) is CH<sub>3</sub>COOH → CH<sub>3</sub>COO+H → CH<sub>3</sub>CO+O+H → CH<sub>2</sub>CO+H+O+H →  
282 CH<sub>2</sub>C+O+H+O+H → CHC+H+O+H+O+H → CC+2H+O+H+O+H, which is similar to the  
283 reported decomposition pathways [36]. The highest energy barrier of 1.19 eV among all  
284 the elementary reactions implies that the decomposition of CHC to CC is the rate-  
285 determining step. It is also found that the decarboxylation of CH<sub>3</sub>COO was suppressed  
286 at the beginning, and hydrogen is released during the whole decomposition process. The  
287 C-C bond is stable throughout the decomposition, and the remaining C-C anchoring on  
288 the Mo facet would result in carbonaceous deposits after further accumulation or they  
289 crack to produce CO<sub>2</sub> & CH<sub>4</sub> with hydrogen and oxygen generated in previous steps [34].

### 290 3.3 FA as hydrogen donor on Mo (110) facet

291 The adsorption energies of FA onto the four different adsorption sites and in four different  
292 configurations are specified in Table 2. The configurations with the binding of O<sup>α</sup>-Mo (①  
293 and ②) showed the highest adsorption energy of 1.15 eV and 0.75 eV respectively.  
294 Configuration with O<sup>β</sup>-Mo led to the adsorption energy of 0.51 eV. Parallel adsorption  
295 (configuration ④) exhibited the lowest adsorption energy of 0.18 eV. Regarding different

296 sites, the adsorption onto the top site led to the highest adsorption energy, followed by  
297 SB, LB and hollow sites with adsorption energies of 0.15 eV, 0.16 eV and 0.12 eV  
298 respectively. These results predict that FA is more likely to adsorb onto the top site of  
299 Mo (110) facet through a single O<sup>α</sup>-Mo (110) bond. EDD was analysed for the adsorption  
300 configurations (①, ②, ③) with high adsorption energies to investigate the interface  
301 interaction, as shown in Fig. 5.

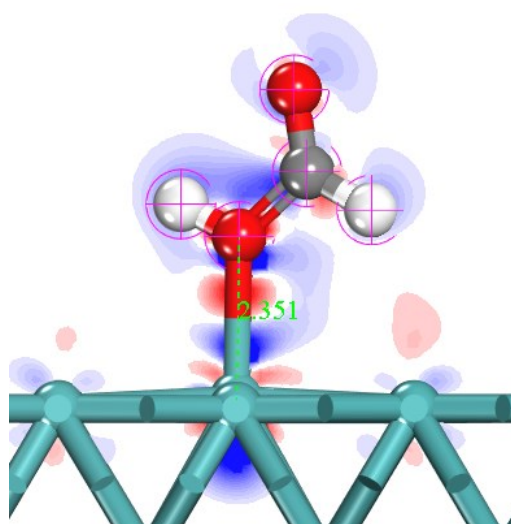


302

(a)

(b)

303



304

(c)

305

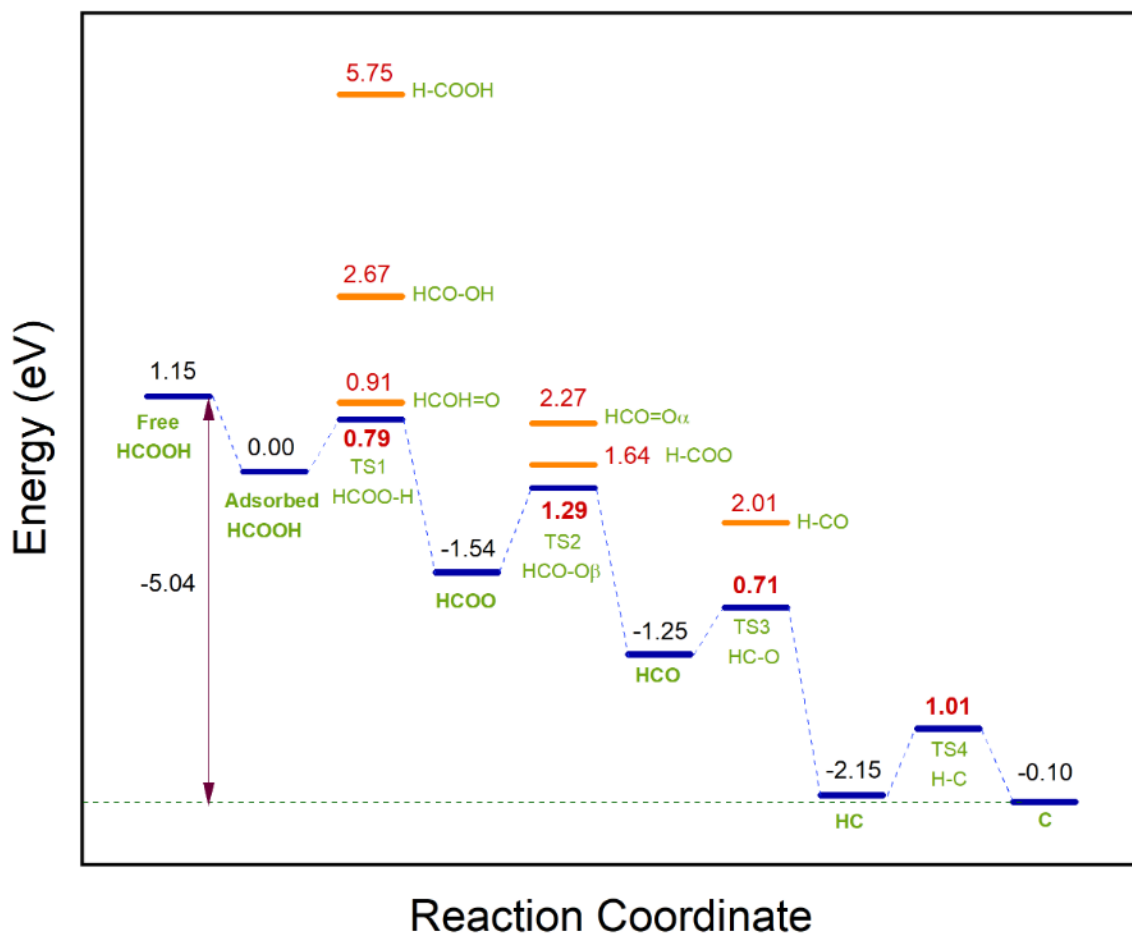


306 Fig. 5. Colour mapping of electron density difference (threshold value: +/- 0.05  
307 electrons/Å<sup>3</sup>) for FA adsorption configurations of (a) Top ①, (b) Top ②, and (c) Top ③  
308 (Loss of electrons is indicated in blue, while electron enrichment is indicated in red)

309 The electron migration exhibited in Fig. 5 indicates that all three adsorption  
310 configurations are in the form of chemisorbed species, where O atom locates at the  
311 centre of electron migration. Significant electrons migration has been observed for the  
312 configuration with O<sup>α</sup>-Mo bond. Fig. 5(a) shows that strong electron lose has taken place  
313 around the O<sup>α</sup>, but apparently electrons were enriched around O<sup>α</sup> and O<sup>β</sup> as well as the  
314 hydroxyl hydrogen atom. Similar but minor electron migrations were also observed in the  
315 other two cases, as demonstrated in Fig. 5 (b) and (c). The strong electron migration  
316 implies large adsorption energy, in line with what has been observed in the AcOH  
317 adsorption. However, AcOH leads to mainly electron lose, while the binding between FA  
318 molecule and Mo (110) facet is found not only results from electron lose, but also from a  
319 strong electron enrichment. This could be ascribed to the electron-donating nature of the  
320 methyl in AcOH molecule.

321 Based on the reaction modelling for the decomposition of FA, the most probable reaction  
322 pathways with the lowest energy barriers are shown in Fig. 6, and the bond lengths and  
323 bond orders for the FA molecule and its most probable intermediates during the  
324 decomposition are presented in Table S4. (a) and (b). The free molecular decomposition  
325 of FA in the absence of metal catalyst is also shown in Fig. 3 for comparison.

326 In the decomposition via the free molecular mechanism, FA showed similar cleavage  
327 energy as AcOH for the bond C<sup>β</sup>-O<sup>α</sup> (8.59 eV), and slightly lower C-H cleavage energy  
328 (4.38 eV) than that of C<sub>α</sub>-H in AcOH. While the bond C-O<sup>β</sup> (4.91 eV) and bond O<sup>β</sup>-H (5.66  
329 eV) were more stable compared to AcOH. All the cleavage reactions in the free molecular  
330 decomposition were endothermic as no new bonds were formed.



331

332

Fig. 6. The decomposition pathways of FA over Mo (110) facet

333 The decomposition of FA over Mo (110) started by the cleavage of O-H with a small  
 334 energy barrier of 0.79 eV, and was followed by the cleavage of the bonds C-O $\beta$  and C=O $\alpha$   
 335 in sequence with energy barriers of 1.29 eV and 0.71 eV respectively. Finally, the C-H  
 336 bond cleaved with an energy barrier of 1.01 eV. All the elementary decomposition  
 337 reactions were exothermic, as shown in Fig. 6.

338 The modelling results confirm that Mo significantly decreases the cleavage energy of  
 339 each bond. For instance, the cleavage energy of hydroxyl O-H bond was lowered from  
 340 5.66 eV in the free molecular decomposition to 0.79 eV over Mo facet. Besides, the  
 341 exothermic property of each step in the catalytic decomposition makes it more  
 342 thermodynamically favoured compared to the free molecular decomposition. The most  
 343 probable decomposition pathway for FA over Mo facet is  $\text{HCOOH} \rightarrow \text{HCOO} + \text{H} \rightarrow$

344  $\text{HCO}+\text{O}+\text{H} \rightarrow \text{HC}+\text{O}+\text{O}+\text{H} \rightarrow \text{H}+\text{C}+\text{O}+\text{O}+\text{H}$ , indicating that O-H and C-H remain the  
345 weakest and strongest bond respectively. The highest energy barrier among the  
346 elementary reactions was 1.29 eV for the C-O<sup>β</sup> cleavage, revealing that it is the rate-  
347 determining step. When O<sup>β</sup> is cleaved, the bond between C and the other oxygen (O<sup>α</sup>) is  
348 weakened significantly with the cleavage energy barrier of only 0.71 eV. The cleavage  
349 of C=O<sup>α</sup> was the exothermic reaction with a significant enthalpy change of 2.15 eV. This  
350 result indicates that the cleavage of the second C-O bond is the most thermodynamically  
351 favoured step for both FA and AcOH. One H atom was released at the beginning of the  
352 FA decomposition process and another one at the final step. The single C atom left on  
353 the Mo facet might result in carbonaceous deposit or CO<sub>2</sub> generation with additional  
354 synthesis reactions [33].

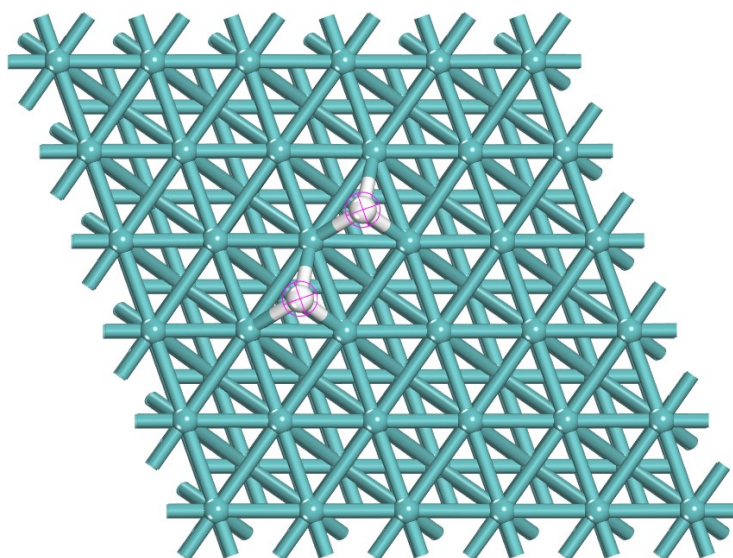
355 The electron migration within the FA molecule under the effect of Mo is not as significant  
356 as that of AcOH. However, the loss of electrons in C=O<sup>α</sup> still makes it cleave easily prior  
357 to C-H bond. The most electron enrichment takes place to the C-O<sup>β</sup> bond, leading to the  
358 highest energy barrier of 1.29 eV for its cleavage reaction.

359 In the catalytic decomposition of AcOH and FA, Mo causes electron migrations between  
360 the interfaces. Consequently most of the bonds in the two acid molecules are significantly  
361 weakened. For instance, it was found that both decompositions start with hydroxyl O-H  
362 cleavage with much cleavage energy compared to the free molecular decomposition.  
363 Besides, the C=O<sup>α</sup> bonds remain to be the strongest bond in both unabsorbed molecules,  
364 but is readily cleaved over Mo facet with much smaller cleavage energy (energy barrier  
365 for catalytic reactions), in comparison with the free molecular decomposition. In presence  
366 of Mo, AcOH can release two H atoms from hydroxyl and methyl group respectively with  
367 low energy barriers, but it requires larger energy to donate another two H atoms from the  
368 methylene; the C-H bond becomes stronger when the C was unsaturated inside the  
369 molecule. In FA decomposition, the hydroxyl hydrogen is also released at the early stage

370 of its decomposition, however it exhibits higher energy barrier compared to the hydroxyl  
371 hydrogen cleavage in AcOH. The other hydrogen in FA is found to be more difficult to  
372 release prior to the cleavage of carboxyl oxygen atom, so that it remains to be the final  
373 step of the decomposition. The modelling results predict that AcOH possesses a better  
374 potential as a hydrogen donor compound over Mo (110) facet.

### 375 3.4 Dissociation of H<sub>2</sub> over Mo (110)

376 The adsorption of H<sub>2</sub> was modelled and the adsorption energy is presented in Table 2.  
377 The results reveal that there were only two possible configurations (vertical and parallel)  
378 and two probable sites (top and hollow) for H<sub>2</sub> adsorption. The adsorption showed similar  
379 adsorption energy in parallel configuration (0.57 eV) and vertical configuration (0.56 eV).  
380 A higher adsorption energy of 1.64 eV resulted from the adsorption onto the hollow  
381 position, which is the only plausible adsorption position observed in the modelling other  
382 than the top position. It is noteworthy that hydrogen molecule was dissociated into two  
383 atoms, anchoring on two hollow positions as shown in Fig. 7, known as dissociative  
384 adsorption [52]. The overall dissociative adsorption process of H<sub>2</sub> remained to be  
385 exothermic.



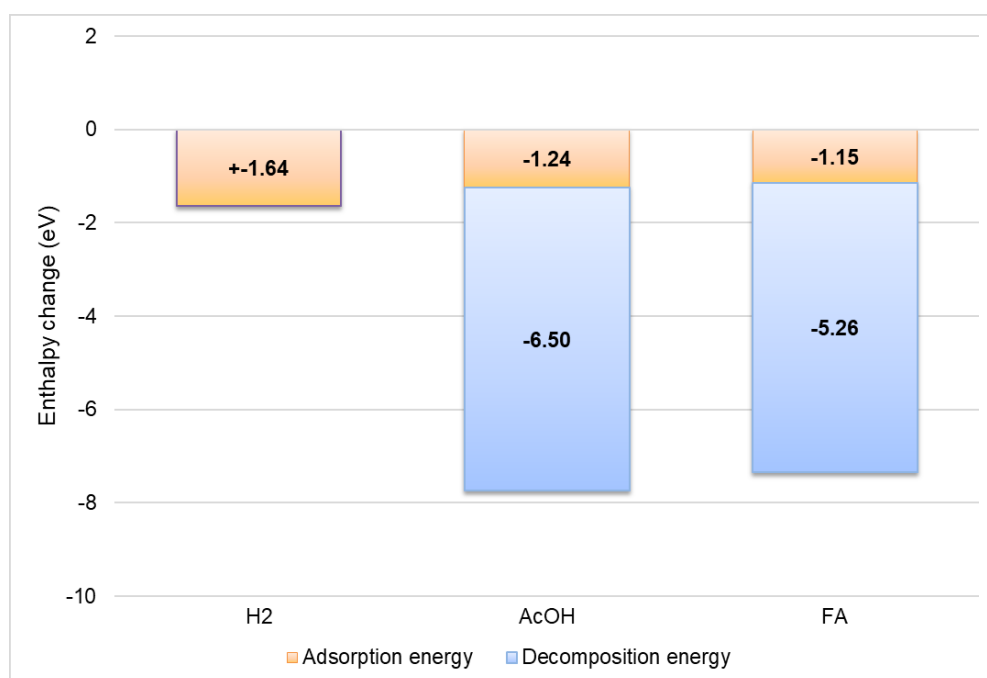
386

387

Fig. 7. Configuration of H<sub>2</sub> adsorption onto hollow position

388 3.5 Comparison of enthalpy changes

389 Modelling results have predicted that the overall decomposition reactions of AcOH and  
390 FA over Mo(110) facet are both exothermic, implying the energy released by new binding  
391 formation between their intermediates and the Mo facet is more than the enthalpy change  
392 for the old binding cleavage [33,36,39]. Thus, the decomposition of both hydrogen  
393 donors over Mo (110) facet is hydrodynamically favoured, similar to the dissociative  
394 adsorption of H<sub>2</sub>. The enthalpy changes for the adsorption and decomposition of AcOH,  
395 FA, and H<sub>2</sub> are calculated respectively, and summarized in Fig. 8.



396

397 Fig. 8. Overall enthalpy change of adsorption and decomposition of hydrogen donor  
398 compounds

399 Hydrogenation and hydrogenolysis reactions normally happen with single hydrogen  
400 migration or spillover during the HDO process [53,54], suggesting that the activation of  
401 single hydrogen atom would be an essential step for the hydrogen donation. Therefore,  
402 the cleavage of metal-single hydrogen bond plays a key role in such a process. The  
403 cleavage (activation) enthalpy of the hydrogen-metal bond is calculated and compared

404 with the adsorption and decomposition enthalpy for each hydrogen donor compound, as  
405 shown in Fig. 8.

406 Additional calculation for the activation of H atom was performed, and the results show  
407 that 3.94 eV was required to activate a single hydrogen atom on Mo (110) facet. Previous  
408 results predicts that the enthalpy change for the dissociative adsorption of hydrogen  
409 molecule is -1.64 eV, which is bigger than those for AcOH and FA (-1.24 eV and -1.15  
410 eV respectively), nevertheless it is inadequate for one single H atom activation. Due to  
411 the exothermic decomposition of AcOH and FA, the overall enthalpy change for the bulk  
412 adsorption and decomposition process of AcOH and FA were -6.50 eV and -6.19 eV  
413 respectively, which are adequate for the activation of H-metal bond. Therefore, the  
414 cleavage of H-metal bond could be more facilitated during the decomposition of AcOH  
415 and FA. In other words, more hydrogen atoms as well as other decomposed atoms would  
416 be likely to migrate and transfer during the decomposition of AcOH and FA compared to  
417 the H<sub>2</sub> gas. In this sense, the bio-acids showed good potential to replace H<sub>2</sub> gas as  
418 alternative hydrogen donors.

#### 419 **4. Conclusions**

420 The performance of AcOH and FA as hydrogen donors over transition metal facets were  
421 investigated and compared with H<sub>2</sub>. The adsorption model showed that facets of Ru  
422 (0001), Mo (110), Ni (111) and Pd (111) led to the strongest binding to the AcOH  
423 molecule among the ten metal facets. Mo (110) was selected as the metal catalyst for  
424 further investigating the hydrogen donation of bio-acids as it is a base metal and the lack  
425 of atomic-level investigation. EDD analyses revealed that the bindings between bio-acids  
426 and Mo were dominated by the electron migration from the molecule to the Mo (110)  
427 facet, while electron enrichments in the acid molecule has also been observed for FA  
428 adsorption. Mo exhibited positive effect on weakening the bond strength for both acids,  
429 and facilitated their cleavage. The reaction model predicted that the most favourable

430 decomposition pathway for acetic acid over Mo (110) was via  $\text{CH}_3\text{COOH} \rightarrow \text{CH}_3\text{COO}+\text{H}$   
431  $\rightarrow \text{CH}_3\text{CO}+\text{O}+\text{H} \rightarrow \text{CH}_2\text{CO}+\text{H}+\text{O}+\text{H} \rightarrow \text{CH}_2\text{C}+\text{O}+\text{H}+\text{O}+\text{H} \rightarrow \text{CHC}+\text{H}+\text{O}+\text{H}+\text{O}+\text{H} \rightarrow$   
432  $\text{CC}+2\text{H}+\text{O}+\text{H}+\text{O}+\text{H}$ , where hydroxyl hydrogen and the methyl hydrogen were more  
433 readily to be released than the H atoms from the unsaturated methylene. The most  
434 favourable decomposition pathway for FA over Mo (110) facet was through  $\text{HCOOH} \rightarrow$   
435  $\text{HCOO}+\text{H} \rightarrow \text{HCO}+\text{O}+\text{H} \rightarrow \text{HC}+\text{O}+\text{O}+\text{H} \rightarrow \text{H}+\text{C}+\text{O}+\text{O}+\text{H}$ , where the hydroxyl hydrogen  
436 can be cleaved and donated at an early stage. Hydrogen showed its undoubtable merits  
437 in hydrogen donation because of its dissociative adsorption property over Mo facet.  
438 However, compared to the decomposition of  $\text{H}_2$  gas, the larger enthalpy change resulted  
439 from the exothermic decomposition of the bio-acid compounds would more benefit the  
440 activation of decomposed atoms from the catalyst surface, including the hydrogen  
441 donation in terms of the single H atom activation and migration. Within the bio-acids,  
442 AcOH exhibited a better potential than FA as a hydrogen donor because it released more  
443 hydrogen atoms with lower energy barriers. The modelling predicted that AcOH has good  
444 potential as an alternative hydrogen donor compound over Mo (110) facet.

## 445 **Author information**

### 446 **Corresponding Authors**

447 X.Z.: [xiaolei.zhang@strath.ac.uk](mailto:xiaolei.zhang@strath.ac.uk)

### 448 **Author Contributions**

449 All the authors have given approval to the final version of the manuscript.

### 450 **Notes**

451 The authors declare no competing financial interest.

## 452 **Acknowledgement**

453 The authors would like to acknowledge financial support from the Leverhulme Trust  
454 Research Grant (RPG-2017-254) and EPSRC First Grant (EP/R010986/1). The authors  
455 are also grateful for computational support from the UK Materials and Molecular  
456 Modelling Hub, which is partially funded by EPSRC (EP/P020194), for which access was  
457 obtained via the UKCP consortium and funded by EPSRC grant ref EP/P022561/1.

## 458 **References**

- 459 [1] K.M. Isa, T.A.T. Abdullah, U.F.M. Ali, *Renew. Sustain. Energy Rev.* 81 (2018)  
460 1259–1268.
- 461 [2] Z. Si, X. Zhang, C. Wang, L. Ma, R. Dong, *Catalysts* 7 (2017) 169.
- 462 [3] Z. Zhang, C. Wang, X. Gou, H. Chen, K. Chen, X. Lu, P. Ouyang, J. Fu, *Appl.*  
463 *Catal. A Gen.* 570 (2019) 245–250.
- 464 [4] M.J. Gilkey, B. Xu, *ACS Catal.* 6 (2016) 1420–1436.
- 465 [5] K.W. Cheah, M.J. Taylor, A. Osatiashtiani, S.K. Beaumont, D.J. Nowakowski, S.  
466 Yusup, A. V. Bridgwater, G. Kyriakou, *Catal. Today* (2019) 1–11.
- 467 [6] Z. Wang, Y. Zeng, W. Lin, W. Song, *Int. J. Hydrogen Energy* 42 (2017) 21040–  
468 21047.
- 469 [7] Y. Zeng, Z. Wang, W. Lin, W. Song, *Chem. Eng. J.* 320 (2017) 55–62.
- 470 [8] T. Guo, Q. Xia, Y. Shao, X. Liu, Y. Wang, *Appl. Catal. A Gen.* 547 (2017) 30–36.
- 471 [9] Y. Wang, S. Agarwal, H.J. Heeres, *ACS Sustain. Chem. Eng.* 5 (2017) 469–480.
- 472 [10] E. Vasiliadou, A. Lemonidou, *Catalysts* 4 (2014) 397–413.
- 473 [11] J. Pajak, V. Krebs, J.F. Maréché, G. Furdin, *Fuel Process. Technol.* 48 (1996) 73–  
474 81.



- 475 [12] D. García-Galindo, M. Gómez-Palmero, M. López-Palmero, E. López, F.  
476 Sebastian, in: 24th Eur. Biomass Conf. Exhib. 6-9 June 2016, Amsterdam,  
477 Netherlands, 2016, pp. 1727–1733.
- 478 [13] H. Shafaghat, P.S. Rezaei, W.M.A.W. Daud, J. Taiwan Inst. Chem. Eng. 65 (2016)  
479 91–100.
- 480 [14] M. Hosseinpour, S. Fatemi, S.J. Ahmadi, M. Morimoto, M. Akizuki, Y. Oshima, E.  
481 Fumoto, Appl. Catal. B Environ. 230 (2018) 91–101.
- 482 [15] Q. Song, F. Wang, J. Cai, Y. Wang, J. Zhang, W. Yu, J. Xu, Energy Environ. Sci.  
483 6 (2013) 994.
- 484 [16] X. Li, G. Chen, C. Liu, W. Ma, B. Yan, J. Zhang, Renew. Sustain. Energy Rev. 71  
485 (2017) 296–308.
- 486 [17] J. Zhang, B. Fidalgo, A. Kolios, D. Shen, S. Gu, Chem. Eng. J. 336 (2018) 211–  
487 222.
- 488 [18] D. Ballesteros-Plata, A. Infantes-Molina, E. Rodríguez-Castellón, Appl. Catal. A  
489 Gen. 580 (2019) 93–101.
- 490 [19] M. Pozzo, D. Alfè, Int. J. Hydrogen Energy 34 (2009) 1922–1930.
- 491 [20] M. Grilc, B. Likozar, Chem. Eng. J. 330 (2017) 383–397.
- 492 [21] S. Ding, Z. Li, F. Li, Z. Wang, J. Li, T. Zhao, H. Lin, C. Chen, Appl. Catal. A Gen.  
493 566 (2018) 146–154.
- 494 [22] B. Hočevar, M. Grilc, M. Huš, B. Likozar, Chem. Eng. J. 359 (2019) 1339–1351.
- 495 [23] J. Zhang, B. Fidalgo, D. Shen, X. Zhang, S. Gu, Mol. Catal. 454 (2018).
- 496 [24] R. Šivec, M. Grilc, M. Huš, B. Likozar, Ind. Eng. Chem. Res. (2019)  
497 acs.iecr.9b00898.

- 498 [25] W. Luo, A. Asthagiri, *J. Phys. Chem. C* 118 (2014) 15274–15285.
- 499 [26] Z.C. Kramer, X.K. Gu, D.D.Y. Zhou, W.X. Li, R.T. Skodje, *J. Phys. Chem. C* 118  
500 (2014) 12364–12383.
- 501 [27] R. ALCALA, *J. Catal.* 218 (2003) 178–190.
- 502 [28] P. Ferrin, D. Simonetti, S. Kandoi, E. Kunkes, J.A. Dumesic, J.K. Nørskov, M.  
503 Mavrikakis, *J. Am. Chem. Soc.* 131 (2009) 5809–5815.
- 504 [29] Y. Choi, P. Liu, *Catal. Today* 165 (2011) 64–70.
- 505 [30] M. Myint, Y. Yan, J.G. Chen, *J. Phys. Chem. C* 118 (2014) 11340–11349.
- 506 [31] F. Gao, Y. Wang, L. Burkholder, C. Hirschmugl, D.K. Saldin, H.C. Poon, D. Sholl,  
507 J. James, W.T. Tysoe, *Surf. Sci.* 602 (2008) 2264–2270.
- 508 [32] K. Kim, J. Oh, T.W. Kim, J.H. Park, J.W. Han, Y.-W. Suh, *Catal. Sci. Technol.* 7  
509 (2017) 3728–3735.
- 510 [33] Z. Jiang, P. Qin, T. Fang, *Appl. Surf. Sci.* 396 (2017) 857–864.
- 511 [34] Y. Huang, X. Dong, Y. Yu, M. Zhang, *J. Phys. Chem. C* 121 (2017) 26733–26741.
- 512 [35] M.D. Esrafil, P. Nematollahi, R. Nurazar, *Synth. Met.* 215 (2016) 164–169.
- 513 [36] X. Li, S. Wang, Y. Zhu, G. Yang, P. Zheng, *Int. J. Hydrogen Energy* 40 (2015)  
514 330–339.
- 515 [37] K.I. Gursahani, R. Alcalá, R.D. Cortright, J.A. Dumesic, *Appl. Catal. A Gen.* 222  
516 (2001) 369–392.
- 517 [38] R. Alcala, J.W. Shabaker, G.W. Huber, M.A. Sanchez-Castillo, J.A. Dumesic, J.  
518 *Phys. Chem. B* 109 (2005) 2074–2085.
- 519 [39] C. Hu, S.-W. Ting, K.-Y. Chan, W. Huang, *Int. J. Hydrogen Energy* 37 (2012)  
520 15956–15965.

521 [40] B. Delley, *J. Chem. Phys.* 92 (1990) 508–517.

522 [41] M.D. Segall, P.J.D. Lindan, M.J. Probert, C.J. Pickard, P.J. Hasnip, S.J. Clark,  
523 M.C. Payne, *J. Phys. Condens. Matter* 14 (2002) 2717–2744.

524 [42] J.P. Perdew, K. Burke, M. Ernzerhof, *Phys. Rev. Lett.* 77 (1996) 3865–3868.

525 [43] S. Grimme, *J. Comput. Chem.* 27 (2006) 1787–1799.

526 [44] K. Lejaeghere, V. Van Speybroeck, G. Van Oost, S. Cottenier, *Crit. Rev. Solid*  
527 *State Mater. Sci.* 39 (2014) 1–24.

528 [45] C.J. Pickard, B. Winkler, R.K. Chen, M.C. Payne, M.H. Lee, J.S. Lin, J.A. White,  
529 V. Milman, D. Vanderbilt, *Phys. Rev. Lett.* 85 (2000) 5122–5125.

530 [46] I.G. Shuttleworth, *Surf. Sci.* 661 (2017) 49–59.

531 [47] F.L. Hirshfeld, *Theor. Chim. Acta* 44 (1977) 129–138.

532 [48] M. Grilc, B. Likozar, *Chem. Eng. J.* 330 (2017) 383–397.

533 [49] J. Zhang, B. Fidalgo, D. Shen, X. Zhang, S. Gu, *Mol. Catal.* 454 (2018) 30–37.

534 [50] A. V. Mironenko, D.G. Vlachos, *J. Am. Chem. Soc.* 138 (2016) 8104–8113.

535 [51] B. Pekmezci Karaman, N. Cakiryilmaz, H. Arbag, N. Oktar, G. Dogu, T. Dogu, *Int.*  
536 *J. Hydrogen Energy* 42 (2017) 26257–26269.

537 [52] J. Greeley, M. Mavrikakis, *J. Phys. Chem. B* 109 (2005) 3460–3471.

538 [53] S. Xia, Z. Yuan, L. Wang, P. Chen, Z. Hou, *Appl. Catal. A Gen.* 403 (2011) 173–  
539 182.

540 [54] A.M. Doyle, S.K. Shaikhutdinov, S.D. Jackson, H.-J. Freund, *Angew. Chemie Int.*  
541 *Ed.* 42 (2003) 5240–5243.

542